

ANALYSIS OF A FOURTH ORDER EXPONENTIAL PDE ARISING FROM A CRYSTAL SURFACE JUMP PROCESS WITH METROPOLIS-TYPE TRANSITION RATES

YUAN GAO, ANYA E. KATSEVICH, JIAN-GUO LIU, JIANFENG LU, AND JEREMY L. MARZUOLA

ABSTRACT. We analytically study a fourth order PDE modelling rough crystal surface diffusion on the macroscopic level. The PDE, originally derived by the second author, is the continuum limit of a microscopic model of the surface dynamics, specified as a Markov jump process with Metropolis type transition rates. We discuss existence of solutions globally in time and long time dynamics for the PDE model. We also outline the derivation of the PDE from the microscopic dynamics, connecting it with previous derivations for dynamics in which the transition rates relate to bond-breaking. In addition, we provide numerical evidence for the convergence to the PDE from the microscopic model as well as numerical studies of the dynamics of the PDE model itself.

1. INTRODUCTION

In this paper, we derive and analyze a fourth order exponential PDE which models the macroscopic dynamics of crystal surface relaxation. The PDE arises as the time and space scaling limit of a microscopic Markov jump process, which evolves via discrete surface hopping events. These events occur at specified transition rates. The transition rates determine the microscopic dynamics, and therefore also shape the macroscopic PDE. Here we primarily focus on transition rates of Metropolis type, meaning that they are a function only of the difference in energy between the pre- and post-jump crystal states.

We also compare the dynamics induced by the Metropolis rates to the dynamics of a generalized Solid-On-Solid (SOS) model, a well-known (and well-studied) model for crystal surface relaxation [Bin83]. This model is remarkable, given its simplicity, for its widespread use in large scale simulations of crystal evolution [PV98]. The SOS model (also known as a broken-bond or bond counting model) uses so-called Arrhenius rates. These rates are functions of the amount of energy needed to break the bonds connecting a particle with its nearest neighbors. Importantly, they do not depend on the configuration of the surface after the jump.

Note that for both sets of rates we use a quadratic interaction potential to define the energy of the system, while the standard SOS model uses an absolute value interaction potential. Under the absolute value potential, the Arrhenius rates simply depend on the number of nearest neighbor bonds at each site. For simplicity however, we still refer to the generalized SOS model with quadratic potential as either the SOS model, broken-bond model, or Arrhenius rate dynamics. We refer to the first dynamics as the Metropolis rate dynamics.

In the continuum limit, we write the crystal surface at a given time $t \geq 0$ as a height profile $h(t, x)$, $x \in \mathbb{T}$, where \mathbb{T} is the unit interval with periodic boundary conditions. The resulting PDE limit we derive here is of the form

$$(1) \quad \partial_t h(t, x) = \partial_x \left(\exp \left[-\partial_x^3 h(t, x) \right] - \exp \left[\partial_x^3 h(t, x) \right] \right), \quad h(0, x) = h_0(x).$$

Conditions on the initial data required for the existence theory will be discussed below.

This PDE has several key features that distinguish it from analogous exponential PDEs derived for the Arrhenius rate dynamics in [MW13, KDM95], and recently revisited in [GLLM19]. The PDE in [KDM95] assumes an absolute value potential, while the PDE in [MW13] is derived using a more general interaction potential, including in particular the quadratic one. For the quadratic potential, it is given by a H^{-1} steepest descent flow of the form

$$(2) \quad \partial_t h = \Delta e^{-\Delta h}, \quad h(0, x) = h_0(x).$$

Recent analytic progress has been made relating to existence of weak solutions, characterization of dynamics, construction of strong solutions, and classification of the breakdown of regularity for this equation. See for instance the works [LX16, LX17, LLMM19, GLL19, Xu18].

In this paper, we develop analytic tools for the PDE (1). In particular, we prove the existence of global solutions to (1) in Section 4. We also explore properties of (1) numerically in Section 5.

One symmetry property of (1) not present in (2) demonstrates an important intrinsic distinction between the microscopic Metropolis and Arrhenius rate dynamics. Namely, if h is a solution to (1) then $-h$ is another solution. This is not the case for (2). In fact, solutions to (2) form singularities in convex regions but not in concave regions [MW13]. Using the structure of the Metropolis and Arrhenius rates, one can show this same symmetry property (or lack thereof) holds on a microscopic level.

The fact that this distinction manifests itself on the macroscopic scale is actually a consequence of the scaling regime under which the limit is taken. For each set of transition rates there are two scaling regimes (i.e. relative scalings of time, space, and height) for which a limiting macroscopic equation exists. Each scaling regime leads to a different PDE. Both here and in [MW13], a non-standard but potentially more informative scaling regime is used to derive (1) and (2), respectively. In another more standard scaling regime, the microscopic versions of the expressions inside the exponentials ($\partial_{xxx}h$ for Metropolis rates and $\partial_{xx}h$ for Arrhenius rates) converge to zero with the scaling parameter, so that one should linearize the exponential to obtain the scaling limit. For both dynamics, this leads to the bi-Laplacian heat flow. In [MW13], the authors show with more careful arguments that the Arrhenius rate process does in fact limit to the bi-Laplacian heat flow in the standard scaling regime. However, deriving the PDE for the Metropolis rate dynamics in this regime has proven difficult, and it is unclear whether the bi-Laplacian heat flow is the correct equation in this case.

Here, we rely on probabilistic arguments in our derivations of the scaling limits. We note however that PDEs corresponding to microscopic processes can also be derived using physical arguments. In [KDM95], for example, the authors use physical principles to derive a PDE for the Arrhenius rate broken bond model with an absolute value potential. The resulting PDE does not have exponential dependence on the derivatives of h , and corresponds to what we referred to above as the standard scaling regime. A separate argument in the last section of [KDM95] suggests an exponential PDE similar to (2) as an alternative. In [KDM95] as well as in [GLLM19], the exponential PDE is obtained by applying the so-called Gibbs-Thomson relation as an underlying approximation for how the density varies with respect to the chemical potential, see [LLMM19], Section 1.1 for details on this approach.

We note that in [KDM95], the authors also derive a PDE for dynamics driven by Metropolis-type rates. This PDE corresponds to the standard scaling regime, whereas the focus of this paper is on the nonstandard regime which leads to an exponential PDE. As mentioned above, using probabilistic arguments to derive the non-exponential PDE in the standard scaling regime has proven to be very difficult.

The derivation of the PDE will closely follow the ideas of [MW13], while attempting to clarify some of the assumptions made about local equilibration of the microscopic dynamics and more carefully establishing some properties of the microscopic processes. The analysis of exponential PDE (1) is another focus of this paper.

The paper will proceed as follows. In Section 2, we describe in detail the family of atomistic models considered in this paper. In Section 3 we provide our derivation of the PDEs and show numerical evidence supporting our claims. In Section 4, we prove the global existence and long time behavior of the solutions to PDE (2). In Section 5, we explore properties of the PDE numerically. In Appendix A we provide supplementary proofs for the convergence argument, and in Appendix B, we give an alternative approach to the analysis of long time dynamics for (1).

Acknowledgements. This project was started while JLM was on sabbatical at Duke University in the Spring of 2019. JLM thanks Bob Kohn, Dio Margetis and Jonathan Weare for many valuable conversations regarding modeling of kinetic Monte Carlo. AEK is supported by the DOE Computational Science Graduate Fellowship. JGL was supported by the National Science Foundation (NSF) grant DMS-1812573 and the NSF grant RNMS-1107444 (KI-Net). JL was supported by the National Science Foundation via grant DMS-1454939. JLM acknowledges support from the NSF through NSF CAREER Grant DMS-1352353.

2. THE MICROSCOPIC MODEL: STATE SPACE AND DYNAMICS

In this section we describe the microscopic dynamics determined by Metropolis-type rates, comparing and contrasting it with the more well-established dynamics given by Arrhenius rates, as in [KDM95, MW13, GLLM19].

2.1. State Space. We represent the microscopic crystal surface of size N as a height profile relative to a fixed level plane, on the lattice torus $\mathbb{T}_N := \mathbb{Z}/N\mathbb{Z}$. The height of the crystal surface at site j is restricted to be an integer h^j , where indices are understood modulo N . A generic profile of length N is denoted by $\mathbf{h}_N = (h^0, \dots, h^{N-1})$. The height gradients corresponding to a profile \mathbf{h} are denoted by $z^i = h^{i+1} - h^i, i = 0, \dots, N-1$. These gradients, rather than the heights themselves, play the key role in the dynamics we study.

To each configuration \mathbf{h} we associate an energy $H(\mathbf{h})$, which depends only on the difference between neighboring heights. Specifically, we have

$$(3) \quad H(\mathbf{h}) = \sum_{i=0}^{N-1} V(z^i), \quad V(z) = z^2.$$

The function $V : \mathbb{Z} \rightarrow \mathbb{R}$ is the interaction potential and represents the energetic cost of changes in height. In general, it is given by a non-negative, strictly convex, symmetric function. Our analysis makes heavy use of the simple algebra of the quadratic potential, and an open question is how to extend the analysis to other common potentials such as $V(z) = |z|^p$.

Note that the energy is invariant under uniform shifts $h^i \mapsto h^i + c, i = 0, \dots, N-1$. We will be interested in dynamics which preserves the total mass $m_N := \sum_{i=0}^{N-1} h^i$ and can therefore eliminate this redundancy by restricting the state space to $\mathbb{Z}_N^m := \{\mathbf{h} \in \mathbb{Z}^N : \sum_{i=0}^{N-1} h^i = m\}$.

We assume the system is in contact with a heat bath at constant temperature T ; thus, the ensemble representing thermal equilibrium is the canonical ensemble. It is given by

$$(4) \quad \rho_N^m(\mathbf{h}) = \frac{1}{\mathcal{Z}} \exp(-\beta H(\mathbf{h})), \quad \mathcal{Z} = \sum_{\mathbf{h} \in \mathbb{Z}_N^m} \exp(-\beta H(\mathbf{h})),$$

where $\beta = \frac{1}{k_B T}$ and k_B is the Boltzmann constant. Because m is fixed throughout, we write ρ_N instead of ρ_N^m below.

2.2. Rates and Reversibility. The dynamics on \mathbb{Z}_N^m is given by a continuous time Markov jump process $\mathbf{h}_N(t) = (h_N^j(t))_{j=0}^{N-1}$. Transitions occur when the top particle at a lattice site i jumps to a neighboring lattice site k ($|i - k| = 1$) with a certain instantaneous transition probability, or rate. We represent the jumps via the operator $J_i^k = J_i \circ J^k$

$$(5) \quad J_i \mathbf{h} = \mathbf{h} - \mathbf{e}_i, \quad J^k \mathbf{h} = \mathbf{h} + \mathbf{e}_k,$$

where \mathbf{e}_j is the j th standard unit vector.

The transitions

$$\mathbf{h} \mapsto J_i^{i\pm 1} \mathbf{h}$$

are the only ones that can occur (have non-zero rate). Note that these transitions preserve the total number of particles m . We denote the rate of the transition $\mathbf{h} \mapsto J_i^j \mathbf{h}$ by $r^{i,j}(\mathbf{h})$.

Since we assume the Markov process has equilibrium measure ρ_N , the rates must satisfy detailed balance with respect to this measure, i.e. one must have

$$(6) \quad \rho_N(\mathbf{h}) r^{i,i+1}(\mathbf{h}) = \rho_N(J_i^{i+1} \mathbf{h}) r^{i+1,i}(J_i^{i+1} \mathbf{h}).$$

Detailed balance ensures that the equilibrium measure ρ_N is stationary under the dynamics determined by the transition rates, and that the resulting stationary process is reversible in time. In other words, under ρ_N the probability that the crystal surface is in state \mathbf{h} and the top particle at site i jumps to the right is equal to the probability that the crystal surface is in state $J_i^{i+1} \mathbf{h}$ and the top particle at site $i+1$ jumps to the left.

The rates considered in [KDM95, MW13, GLLM19] are the so-called Arrhenius rates of the SOS model. They are symmetric with respect to jumping left and right, and are given by

$$(7) \quad r_{\text{Arr}}^i(\mathbf{h}) = r_{\text{Arr}}^{i,\pm 1}(\mathbf{h}) := \frac{1}{2} \exp[-\beta(H(J_i \mathbf{h}) - H(\mathbf{h}))].$$

One can check that these rates satisfy the detailed balance equation (6) by exponentiating the equality

$$-\beta H(\mathbf{h}) - \beta [H(J_i \mathbf{h}) - H(\mathbf{h})] = -\beta H(J_i \mathbf{h}) = -\beta H(J_i^{i+1} \mathbf{h}) - \beta [H(J_{i+1} J_i^{i+1} \mathbf{h}) - H(J_i^{i+1} \mathbf{h})].$$

The expression in the exponent of the Arrhenius rates is the energy cost associated with removing a single atom from site i on the crystal surface. Once the bonds with its neighbors are broken, the atom jumps either left or right with probability $\frac{1}{2}$. The symmetry of the Arrhenius rates simplifies the calculation of the mobility, which is the response of the microscopic system to a small external field and appears in the PDE limit in [KDM95]. In our PDE limit a term similar to the mobility also arises. For more detail, see the discussion at the end of Section 3.3.

Using the definition of the Hamiltonian, we also write the rates explicitly in terms of the height gradients z_i . The only gradients affected by the removal of a particle at site i are z^{i-1} , which decreases by 1, and z^i , which increases by 1. Thus

$$(8) \quad r_{\text{Arr}}^i(\mathbf{h}) = \frac{1}{2} \exp \left[-\beta \left((z^{i-1} - 1)^2 + (z^i + 1)^2 - (z^{i-1})^2 - (z^i)^2 \right) \right] = \frac{1}{2} e^{-2\beta} \exp[-2\beta(z^i - z^{i-1})].$$

The new set of rates considered in this work are of Metropolis type, by which we mean any set of rates which satisfy detailed balance with respect to ρ_N and which are functions only of the difference in energy between the pre- and post-jump crystal states. The specific rates we consider are

$$(9) \quad r_{\text{Met}}^{i,j}(\mathbf{h}) := \exp \left[-\frac{\beta}{2} (H(J_i^j \mathbf{h}) - H(\mathbf{h})) \right], \quad j = i \pm 1.$$

Detailed balance follows from

$$-\beta H(\mathbf{h}) - \frac{\beta}{2} [H(J_i^{i+1} \mathbf{h}) - H(\mathbf{h})] = -\frac{\beta}{2} [H(J_i^{i+1} \mathbf{h}) + H(\mathbf{h})] = -\beta H(J_i^{i+1} \mathbf{h}) - \frac{\beta}{2} [H(\mathbf{h}) - H(J_i^{i+1} \mathbf{h})].$$

These rates give preference to atomistic motion that lowers the surface energy H . Importantly, the dynamics is not symmetric with respect to jumping left or right, instead favoring the direction yielding lower energy.

Another common set of Metropolis-type rates is given by $r^{i,j}(\mathbf{h}) = \exp[-\beta(H(J_i^j \mathbf{h}) - H(\mathbf{h}))] \wedge 1$. These are the rates considered in [KDM95] (in addition to Arrhenius rates). See also [KMV03] and works cited there for a discussion of the Metropolis rates in the context of coarse-grained stochastic processes. We note that while $e^{-\Delta H} \wedge 1$ is also the acceptance probability in standard Metropolis-Hastings algorithms, the goal of that algorithm is to sample the invariant Gibbs measure, whereas we are interested in the Markov process dynamics itself. We chose rates of the form $\exp[-\Delta H/2]$ due to their analytic tractability. In our derivation of the scaling limit, we will need to compute expectations $\langle r^{i,j}(\mathbf{h}) \rangle$, and this is more straightforward for these rates than for the Metropolis rates involving a minimum.

The height gradients affected by a jump from site i to site $i+1$ are z^{i-1} and z^{i+1} , which decrease by 1, and z^i , which increases by 2. Therefore, $r_{\text{Met}}^{i,i+1}(\mathbf{h})$ can be written in terms of the gradients as

$$(10) \quad \begin{aligned} r_{\text{Met}}^{i,i+1}(\mathbf{h}) &= \exp \left(-\frac{\beta}{2} \left((z^{i-1} - 1)^2 + (z^i + 2)^2 + (z^{i+1} - 1)^2 - (z^{i-1})^2 - (z^i)^2 - (z^{i+1})^2 \right) \right) \\ &= e^{-3\beta} \exp(-\beta(z^{i-1} - 2z^i + z^{i+1})). \end{aligned}$$

Similarly,

$$(11) \quad r_{\text{Met}}^{i+1,i}(\mathbf{h}) = e^{-3\beta} \exp(\beta(z^{i-1} - 2z^i + z^{i+1})).$$

2.3. Markov Process Generator. The rates fully specify the dynamics via the generator \mathcal{A} , an operator acting on observables f of the Markov process. The generator quantifies the instantaneous change in the average value of the observable through the evolution equation

$$(12) \quad f(\mathbf{h}(t)) = f(\mathbf{h}(0)) + \int_0^t (\mathcal{A}f)(\mathbf{h}(s)) ds + M_f(t),$$

where $M_f(t)$ is a mean zero martingale.

The generator is given by

$$(13) \quad (\mathcal{A}f)(\mathbf{h}) = \sum_{i=0}^{N-1} r^{i,i+1}(\mathbf{h}) (f(J_i^{i+1}\mathbf{h}) - f(\mathbf{h})) + r^{i+1,i}(\mathbf{h}) (f(J_{i+1}^i\mathbf{h}) - f(\mathbf{h})).$$

Specially, let $\pi^i(\mathbf{h}) = h^i$ be the projection operator onto h^i . Using (13) with $f = \pi^i$, we see that

$$\mathcal{A}\pi^i(\mathbf{h}) = (r^{i-1,i} - r^{i,i-1})(\mathbf{h}) - (r^{i,i+1} - r^{i+1,i})(\mathbf{h}).$$

Let $\mathcal{J}^{i,i+1}(\mathbf{h}) = (r^{i,i+1} - r^{i+1,i})(\mathbf{h})$, which represents the expected net instantaneous current from site i to site $i + 1$. We may then write

$$\mathcal{A}\pi^i(\mathbf{h}) = \mathcal{J}^{i-1,i}(\mathbf{h}) - \mathcal{J}^{i,i+1}(\mathbf{h}).$$

Using (12) in differential form, we obtain

$$(14) \quad dh^i(t) = [\mathcal{J}^{i-1,i}(\mathbf{h}_N(t)) - \mathcal{J}^{i,i+1}(\mathbf{h}_N(t))] dt + dM^i(t).$$

This equation is the microscopic, stochastic form of a conservation law expressing the change in height at site i as the negative divergence of current.

3. MACROSCOPIC SCALING LIMITS

In this section we define the scaling limit and discuss local equilibration, a key assumption in our derivation. We then give a non-rigorous theoretical argument for the scaling limit and confirm the result with numerical experiments. The simulations also confirm unproven claims made in the argument.

3.1. Scaling & Local Equilibration. We shall obtain a macroscopic profile $h(x, t), x \in \mathbb{T}$, as a limit of the process

$$\bar{\mathbf{h}}_N(t) = N^{-q_1} \mathbf{h}_N(N^{q_2}t),$$

a rescaled version of the original microscopic process. Thus we slow time down by N^{q_2} and scale height down by N^{q_1} . We will associate the j th site with the interval $(j/N, (j+1)/N)$, so that the space domain is scaled down by N .

We will see that for both Arrhenius rate and Metropolis rate dynamics, we must take $q_2 = 4$ in order to obtain a limit that does not blow up or get annihilated. For both sets of rates, there is a range of choices for q_1 which yield a limit. However, there is only one value of q_1 ($q_1 = 2$ for Arrhenius rates and $q_1 = 3$ for Metropolis rates) which yields a PDE with an exponential nonlinearity. We will keep q_1 and q_2 unspecified for most of the discussion below, and at the end of the argument it will become clear why they must take these particular values. We note that in the standard scaling regime alluded to in the introduction, one takes $q_1 = 1$ for both sets of rates.

In the spirit of statistical mechanics, the macroscopic profile $h(x, t)$ should not be affected by changes to any single individual height h_N^j . We therefore define convergence through the lens of weighted averages, i.e. integrals against functions $\phi \in C_0^\infty(\mathbb{T})$. It will be useful to think of $\bar{\mathbf{h}}_N(t)$ as a random signed measure $\bar{h}_N(dx, t)$ supported on \mathbb{T} or equivalently, as a step function $\bar{h}_N(x, t), x \in \mathbb{T}$:

$$(15) \quad \begin{aligned} \bar{h}_N(dx, t) &= \frac{1}{N} \sum_{j=0}^{N-1} N^{-q_1} h_N^j(N^{q_2}t) \delta\left(x - \frac{j}{N}\right) \\ &\Leftrightarrow \\ \bar{h}_N(x, t) &= N^{-q_1} h_N^{\lfloor Nx \rfloor}(N^{q_2}t). \end{aligned}$$

Taking the former viewpoint, we define convergence as follows:

Definition 3.1. *We say that the random variable $\bar{\mathbf{h}}_N(t) = N^{-q_1} \mathbf{h}_N(N^{q_2}t)$ converges to $h(x, t)$ if*

$$(\phi, \bar{h}_N(t, \cdot)) := \frac{1}{N} \sum_{j=0}^{N-1} N^{-q_1} h_N^j(N^{q_2}t) \phi(j/N) \rightarrow \int_{\mathbb{T}} h(x, t) \phi(x) dx$$

in probability as $N \rightarrow \infty \quad \forall \phi \in C_0^\infty(\mathbb{T})$.

In Section 3.2 we show that if $\bar{\mathbf{h}}_N(t)$ converges to some $h(x, t)$ for all $t \geq 0$, then h must satisfy a certain PDE which depends on the choice of q_1, q_2 and the rates (Arrhenius or Metropolis). We will not however prove that $\bar{\mathbf{h}}_N(t)$ does in fact have a limit.

Our argument depends critically on the assumption that, after a macroscopically negligible amount of time, the measure of the process can be well approximated by a certain local equilibrium measure called the optimal twist. By local equilibrium, we mean a distribution in which macroscopically local averages of $\mathbf{h}_N(t)$ in space or time (i.e. space-time integrals against smooth functions $\phi(x, t)$ compactly supported in $\mathbb{T} \times (0, \infty)$) are approximately equal to their expected values. The optimal twist is one such measure.

Hypothesis 3.2 (Optimal Twist). *As $N \rightarrow \infty$, the measure of $\mathbf{h}_N(N^{q_2}t)$ is increasingly well approximated by a measure $p_{\lambda_N(t)}$ in the family of optimal twist measures*

$$(16) \quad \left\{ p_{\lambda} \mid \lambda \in \mathbb{R}^N, \quad \text{supp}(p_{\lambda}) = \mathbb{Z}_N^m, \quad p_{\lambda}(\mathbf{h}) = \frac{1}{\mathcal{Z}_{\lambda}} \prod_{i=0}^{N-1} \exp\left(-\beta(z^i)^2 + \lambda^i z^i\right) \right\},$$

where \mathcal{Z}_{λ} is a normalization constant. Specifically, $\lambda_N(t)$ is determined by the implicit equations

$$(17) \quad \langle z^i \rangle_{\lambda_N(t)} = N^{q_1-1} \partial_x h\left(\frac{i}{N}, t\right), \quad i = 0, \dots, N-1,$$

where $\langle \cdot \rangle_{\lambda}$ denotes expectation with respect to p_{λ} and h is the assumed macroscopic limit of $\bar{\mathbf{h}}_N$.

Note the time parametrization, $\mathbf{h}_N(N^{q_2}t) \sim p_{\lambda_N(t)}$, which indicates that the measure evolves on the macroscopic time scale. The optimal twist measure is the solution to the minimization problem

$$p_{\lambda_N(t)} = \arg \min_{\mu \in S} H(\mu \mid \rho_N), \quad S = \{\mu \mid \langle z^i \rangle_{\mu} = N^{q_1-1} \partial_x h(i/N, t), \quad \forall i = 0, \dots, N-1\},$$

where H is relative entropy:

$$H(\mu \mid \nu) = \sum_{\mathbf{h} \in \mathbb{Z}_N^m} \mu(\mathbf{h}) \log(\mu(\mathbf{h})/\nu(\mathbf{h})).$$

In other words, $p_{\lambda_N(t)}$ is the closest measure to global equilibrium under which the expected values of the slopes z^i match their macroscopic counterpart, where λ_N can be viewed as a biasing potential for the microscopic ensemble so that the match occurs. The N^{q_1-1} scaling in (17) comes from the following: if $h(i/N, t) \approx N^{-q_1} \langle h_N^i(N^{q_2}t) \rangle$ then, omitting the time variable for simplicity,

$$\partial_x h\left(\frac{i}{N}\right) \approx N \left(h\left(\frac{i+1}{N}\right) - h\left(\frac{i}{N}\right) \right) \approx N^{1-q_1} \langle h_N^{i+1} - h_N^i \rangle = N^{1-q_1} \langle z^i \rangle.$$

Consider the definition of p_{λ} in (16). It is a product measure of the slopes z^i conditioned on $\mathbf{h} \in \mathbb{Z}_N^m$. For large N , one expects to induce negligible error by considering the z^i to be independent (this is for now an assumption, but these errors will be analyzed in future work). In this case, the equations (17) break up into N independent equations, and we have

$$\lambda_i(t) = \lambda(N^{q_1-1} \partial_x h(i/N, t)),$$

where $\lambda(u)$ is defined implicitly via

$$u = \frac{\sum_{n \in \mathbb{Z}} n e^{-\beta n^2 + \lambda(u)n}}{\sum_{n \in \mathbb{Z}} e^{-\beta n^2 + \lambda(u)n}} =: \langle z \rangle_{\lambda},$$

where $\langle \cdot \rangle_{\lambda}$ denotes expectation with respect to $p_{\lambda}(n) \propto e^{-\beta n^2 + \lambda n}$, $n \in \mathbb{Z}$.

In [MW13], it is shown that $\lambda(N^{\alpha}u) = O(N^{\alpha})$, and if $\alpha > 0$ then

$$\lambda(N^{\alpha}u)/N^{\alpha} \rightarrow 2\beta u, \quad N \rightarrow \infty.$$

In Section 3.3 we verify numerically that Hypothesis 3.2 is correct for the Arrhenius rates, and approximately valid for the Metropolis rates. There is reason to believe that for asymmetric rates such as the Metropolis rates, the true measure is not fully captured by the optimal twist as $N \rightarrow \infty$. The dynamics of the macroscopic PDE we obtain by assuming the optimal twist is nevertheless extremely close to the true dynamics. See the discussion at the end of Section 3.3.

3.2. Scaling Limit: Theory. In this section we state and give a heuristic argument for the macroscopic scaling limit.

Proposition 3.3. *Assume $\bar{\mathbf{h}}_N(t) = N^{-q_1} \mathbf{h}_N(N^{q_2}t)$ converges to some smooth function $h(x, t)$ for all $t \geq 0$, where convergence is defined as in Definition 3.1, and $\mathbf{h}_N(t)$ is the Markov jump process determined by the Arrhenius or Metropolis rates. Assume also the Optimal Twist Hypothesis 3.2. Then h satisfies the conservation equation*

$$(18) \quad \partial_t h = \partial_x (\mathcal{D}h),$$

where for $q_1 = 2, q_2 = 4$ and Arrhenius rate dynamics we have $\mathcal{D} = \mathcal{D}_{Arr}$,

$$(19) \quad \mathcal{D}_{Arr}h = -\frac{1}{2}\partial_x (e^{-2\beta\partial_{xx}h}) = \beta(\partial_{xxx}h)e^{-2\beta\partial_{xx}h},$$

while for $q_1 = 3, q_2 = 4$ and Metropolis rate dynamics we have $\mathcal{D} = \mathcal{D}_{Met}$,

$$(20) \quad \mathcal{D}_{Met}h = e^{-\frac{3}{2}\beta} (e^{-\beta\partial_{xxx}h} - e^{\beta\partial_{xxx}h}).$$

We will need the following lemmas, proved in the appendix. Recall the definition of current between sites, for generic rates:

$$\mathcal{J}^{i,i+1} = r^{i+1,i} - r^{i,i+1}.$$

Lemma 3.4. *For any rates in detailed balance with the global equilibrium measure ρ_N , and for any measure p_λ in the optimal twist family, we have*

$$(21) \quad \langle \mathcal{J}^{i,i+1} \rangle_\lambda = (1 - \exp(-\lambda^{i-1} + 2\lambda^i - \lambda^{i+1})) \langle r^{i,i+1} \rangle_\lambda.$$

In the proof of Proposition 3.3, we will apply (21) for $\lambda = \lambda_N(t)$. Recall that $\lambda_N^i(t) \approx 2\beta N^{q_1-1} \partial_x h(i/N, t)$ for large N .

Lemma 3.5. *For the Arrhenius rates,*

$$(22) \quad \langle r_{Arr}^{i,i+1} \rangle_{\lambda_N(t)} = \frac{1}{2} \exp(-(\lambda_N^i(t) - \lambda_N^{i-1}(t))) \approx \frac{1}{2} \exp(-2\beta N^{q_1-2} \partial_{xx} h(i/N, t))$$

For the Metropolis rates,

$$(23) \quad \begin{aligned} \langle r_{Met}^{i,i+1} \rangle_{\lambda_N(t)} &\approx e^{-\frac{3}{2}\beta} \exp\left(\frac{1}{2}(\lambda_N^{i-1}(t) - 2\lambda_N^i(t) + \lambda_N^{i+1}(t))\right) \\ &\approx e^{-\frac{3}{2}\beta} \exp(\beta N^{q_1-3} \partial_{xxx} h(i/N, t)). \end{aligned}$$

Remark 3.6. *The exact expression for the Metropolis rate expectation involves an additional multiplicative factor depending on β and λ_N^i . When β is small, it is approximately given by $1 + 4e^{-\pi^2/\beta} \cos(\lambda_N^i \pi/\beta)$. This factor is nearly equal to one for the values of β we consider in our numerical simulations ($\beta \leq 0.25$). We therefore disregard it below.*

Proof of Proposition 3.3. We give an informal argument which clearly and easily shows how the operator \mathcal{D} arises from the microscopic dynamics. A slightly more formal argument is given in the appendix.

Recall the stochastic conservation law for the microscopic heights (14), given by the finite difference of the microscopic current $\mathcal{J}^{i,i+1}(\mathbf{h}_N)$. The proposed PDE is also a conservation law, and we may think of $\mathcal{D}h$ as the macroscopic current. Roughly speaking, our task is therefore to express the microscopic current as a discrete differential operator acting on \mathbf{h}_N . The continuous limit of this operator will be our desired \mathcal{D} .

We begin by writing the stochastic conservation law of the rescaled process $\bar{\mathbf{h}}_N(t)$ using (14). We have

$$d\bar{h}_N^i(t) = N^{-q_1} dh_N^i(N^{q_2}t) = N^{q_2-q_1} [\mathcal{J}^{i-1,i}(\mathbf{h}_N(N^{q_2}t)) - \mathcal{J}^{i,i+1}(\mathbf{h}_N(N^{q_2}t))] dt + dM^i(N^{q_2}t).$$

Arguing that the process varies smoothly in space, we must have that $M^i(N^{q_2}t)$ approximately equals the average of $M^j(N^{q_2}t)$ over j in a window centered at i . Using the local equilibration hypothesis, this spatial average approximately equals its expectation, which is zero. We can therefore neglect the martingale term. Thus,

$$d\bar{h}_N^i(t) \approx N^1 (N^{q_2-q_1-1} \mathcal{J}^{i-1,i} - N^{q_2-q_1-1} \mathcal{J}^{i,i+1}) (\mathbf{h}_N(N^{q_2}t)) dt,$$

or in integral form,

$$(24) \quad \bar{h}_N^i(t + \epsilon) - \bar{h}_N^i(t) \approx \int_t^{t+\epsilon} N^1 (N^{q_2 - q_1 - 1} \mathcal{J}^{i-1, i} - N^{q_2 - q_1 - 1} \mathcal{J}^{i, i+1}) (\mathbf{h}_N(N^{q_2} s)) ds$$

The integral in (24) is a (macroscopically) local time average and, assuming the onset of local equilibrium, can therefore be replaced with its expectation. Assuming Hypothesis 3.2, the distribution of the process is approximated by the optimal twist measure. Combined, these assumptions imply

$$(25) \quad \bar{h}_N^i(t + \epsilon) - \bar{h}_N^i(t) \approx \int_t^{t+\epsilon} N^1 (\langle N^{q_2 - q_1 - 1} \mathcal{J}^{i-1, i}(\mathbf{h}) \rangle_{\lambda_N(s)} - \langle N^{q_2 - q_1 - 1} \mathcal{J}^{i, i+1}(\mathbf{h}) \rangle_{\lambda_N(s)}) ds.$$

The integrand is now nonrandom and must limit to the right hand side of the PDE we will obtain. We show that if q_1 and q_2 are chosen appropriately, the expression $\langle N^{q_2 - q_1 - 1} \mathcal{J}^{i, i+1}(\mathbf{h}) \rangle_{\lambda_N(t)}$ has an $O(1)$ limit. Since the integrand is a finite difference of this expression, it will become a space derivative in the limit, and we must therefore have

$$(\mathcal{D}h)(x, t) = \lim_{N \rightarrow \infty} \langle N^{q_2 - q_1 - 1} \mathcal{J}^{i, i+1}(\mathbf{h}) \rangle_{\lambda_N(t)}.$$

Recall the expression for the current expectation $\langle \mathcal{J}^{i, i+1}(\mathbf{h}) \rangle_{\lambda}$ given in Lemma 3.4:

$$\langle \mathcal{J}^{i, i+1} \rangle_{\lambda} = (1 - \exp(-\lambda^{i-1} + 2\lambda^i - \lambda^{i+1})) \langle r^{i, i+1} \rangle_{\lambda}.$$

Because of the different forms of the Arrhenius and Metropolis rate expectations, we now consider the two dynamics separately. In particular, we will see how the form of the rate expectation influences the choice of q_1 .

Arrhenius rates: Recall that the Arrhenius rate expectation (22) is given by

$$\langle r_{Arr}^{i, i+1} \rangle_{\lambda_N(t)} \approx \frac{1}{2} \exp(-2\beta N^{q_1 - 2} \partial_{xx} h(i/N, t))$$

for large N . Thus, to retain this exponential in the PDE, we must take $q_1 = 2$. Since $\lambda^i = O(N^{q_1 - 1})$, we have $\lambda^{i-1} - 2\lambda^i + \lambda^{i+1} = O(N^{q_1 - 3}) = O(N^{-1})$. Therefore, the first part of the expression for the current expectation is given by

$$(26) \quad 1 - \exp(-\lambda^{i-1}(t) + 2\lambda^i(t) - \lambda^{i+1}(t)) \approx \lambda^{i-1}(t) - 2\lambda^i(t) + \lambda^{i+1}(t) \approx 2\beta N^{-1} \partial_{xxx} h(i/N, t).$$

Multiplying the above two factors and substituting $q_1 = 2$, we obtain

$$(27) \quad N^{q_2 - q_1 - 1} \langle \mathcal{J}^{i, i+1} \rangle_{\lambda} = N^{q_2 - 4} \beta \partial_{xxx} h(i/N, t) \exp(-2\beta \partial_{xx} h(i/N, t)).$$

We see that we must have $q_2 = 4$ to obtain a macroscopic limit. Taking $N \rightarrow \infty$, we obtain $\mathcal{D}_{Arr} h$ as in (19).

Metropolis rates: Recall that the Metropolis rate expectation (23) is given by

$$\langle r_{Met}^{i, i+1} \rangle_{\lambda_N(t)} \approx e^{-\frac{3}{2}\beta} \exp(\beta N^{q_1 - 3} \partial_{xxx} h(i/N, t))$$

for N large. Thus, to retain this exponential in the PDE, we must take $q_1 = 3$. Then the first term in the expression for the current is given by

$$(28) \quad 1 - \exp(-\lambda^{i-1}(t) + 2\lambda^i(t) - \lambda^{i+1}(t)) \approx 1 - \exp(-2\beta \partial_{xxx} h(i/N, t)).$$

Multiplying the above two factors and substituting $q_1 = 3$, we obtain

$$(29) \quad \begin{aligned} N^{q_2 - q_1 - 1} \langle \mathcal{J}^i \rangle_{\lambda} &= N^{q_2 - 4} (1 - \exp(-2\beta \partial_{xxx} h(i/N, t))) e^{-\frac{3}{2}\beta} \exp(\beta \partial_{xxx} h(i/N, t)) \\ &= N^{q_2 - 4} e^{-\frac{3}{2}\beta} \left(e^{\beta \partial_{xxx} h(i/N, t)} - e^{-\beta \partial_{xxx} h(i/N, t)} \right). \end{aligned}$$

We see that we must have $q_2 = 4$ to obtain a macroscopic limit. Taking $N \rightarrow \infty$, we obtain $\mathcal{D}_{Met} h$ as in (20). \square

3.3. Scaling Limit: Numerics. Our numerical simulations have two primary aims: (1) to determine whether the PDEs we obtained accurately model the evolution of the rescaled microscopic process $\bar{\mathbf{h}}_N(t)$ as $N \rightarrow \infty$, and (2) to confirm the form of the local equilibrium measure we assumed of the microscopic model.

Methods.

To solve the PDE, we discretized spatially using centered difference schemes and applied a numerical ODE timestepper designed for stiff ODEs. To simulate the microscopic process, we used the Kinetic Monte Carlo (KMC) method. In this method, one iteratively updates the state of the process, $\mathbf{h} \mapsto \mathbf{h}'$, and the physical time, $t \mapsto t + \Delta$ until the desired final time is reached. The new state \mathbf{h}' is randomly chosen with probability proportional to the transition rate $r(\mathbf{h} \mapsto \mathbf{h}')$, and Δ , which represents the amount of time the process spent in state \mathbf{h} , is chosen from an exponential distribution $\text{Exp}(\lambda)$, with $\lambda = \sum_{\mathbf{h}'} r(\mathbf{h} \mapsto \mathbf{h}')$.

To compare the macroscopic and rescaled microscopic processes, we fix an initial non-trivial (out of equilibrium) macroscopic profile $h(x, 0) = h_0(x)$ for which $\|h\|_\infty > 0$ in order to ensure non-trivial dynamics in both the microscopic and macroscopic flows. We evolve the PDE forward from h_0 to some macroscopic times of interest T . Then, for various N , we run KMC from the initial microscopic profile $\mathbf{h}_N(0) = (N^{q_1} h_0(j/N))_{j=0}^{N-1}$ (where $q_1 = 2$ for Arrhenius rate dynamics and $q_1 = 3$ for Metropolis rate dynamics) up to the microscopic time $N^4 T$. We should then expect to see that $h(j/N, T) \approx N^{-q_1} h_N^j(N^4 T)$ for large N .

We also check the primary local equilibration assumption used in the PDE derivation, namely, that macroscopically local in time averages of observables of $\mathbf{h}_N(t)$ can be replaced by their expectation with respect to the optimal twist. The observable whose time- and distribution average we choose to compare is the rate function, since it is the one appearing in the derivation. Specifically, we check whether

$$(30) \quad \langle r^{i,i+1}(\mathbf{h}) \rangle_{\lambda_N(T)} \approx \frac{1}{2N^4 \delta} \int_{N^4(T-\delta)}^{N^4(T+\delta)} r^{i,i+1}(\mathbf{h}_N(s)) ds.$$

The left hand side is computed using formulas (22) and (23) for the optimal twist expectation of the Arrhenius and Metropolis rates, respectively. The parameter $\lambda_N(t)$ is a function of the macroscopic profile $h(x, t)$, which we estimate using the PDE solution.

The right hand side is the integral of a step function, since the microscopic process is a Markov jump process. It can therefore be simply computed from the KMC simulation by keeping track of the rate values and time between jumps.

For the Metropolis rate dynamics, we consider two initial profiles and values of β : $h_0(x) = \frac{1}{10} \sin(2\pi x)$, with $\beta = 0.25$ and $h_0(x) = g(x) + g(x + 0.2 \bmod 1)$ with $\beta = 0.01$, where

$$g(x) = \frac{1}{10} \exp\left(8 - 1/x - 1/\left(\frac{1}{2} - x\right)\right) \mathbb{1}_{(0, \frac{1}{2})}(x)$$

is a smooth bump function supported on $(0, \frac{1}{2})$. For the Arrhenius rate dynamics, we take $h_0(x) = \frac{1}{10} \sin(2\pi x)$, with $\beta = 1.5$. The reason for choosing small amplitude for the initial profile and small β is to limit how large the rates can be, since they depend exponentially on β and the curvature of \mathbf{h}_N .

Results.

Figure 1 shows results from the experiment with a compactly supported two-bump initial profile, and $\beta = 0.01$. We observe an excellent fit of the PDE solution to the microscopic profile obtained from KMC. The top left figure shows that on the scale of the initial height amplitude, the PDE dynamics exactly coincides with the microscopic dynamics for $N = 200$. The top right figure shows that the PDE also fits the microscopic dynamics on the scale of small shifts in amplitude. Moreover, the microscopic dynamics (after rescaling) has already converged for $N = 400$, since increasing N does not affect the dynamics.

The bottom left (bottom right) figure compares the time average of the right-jump rates (left-jump rates) with its expectation with respect to the optimal twist measure, as in (30). The figures show that the optimal twist assumption seems to hold. The zoomed-in part of the plot shows that the KMC rate time average oscillates more closely around the optimal twist expectation as N increases.

Figure 2 shows results from the experiment with a sinusoidal initial profile and $\beta = 0.25$. Qualitatively, the PDE fully captures the microscopic dynamics. However, compared to the two-bump initial profile, we observed a slightly poorer fit between the PDE and microscopic dynamics. The top right and bottom figures, in which results from different values of N are presented, show that the microscopic process has

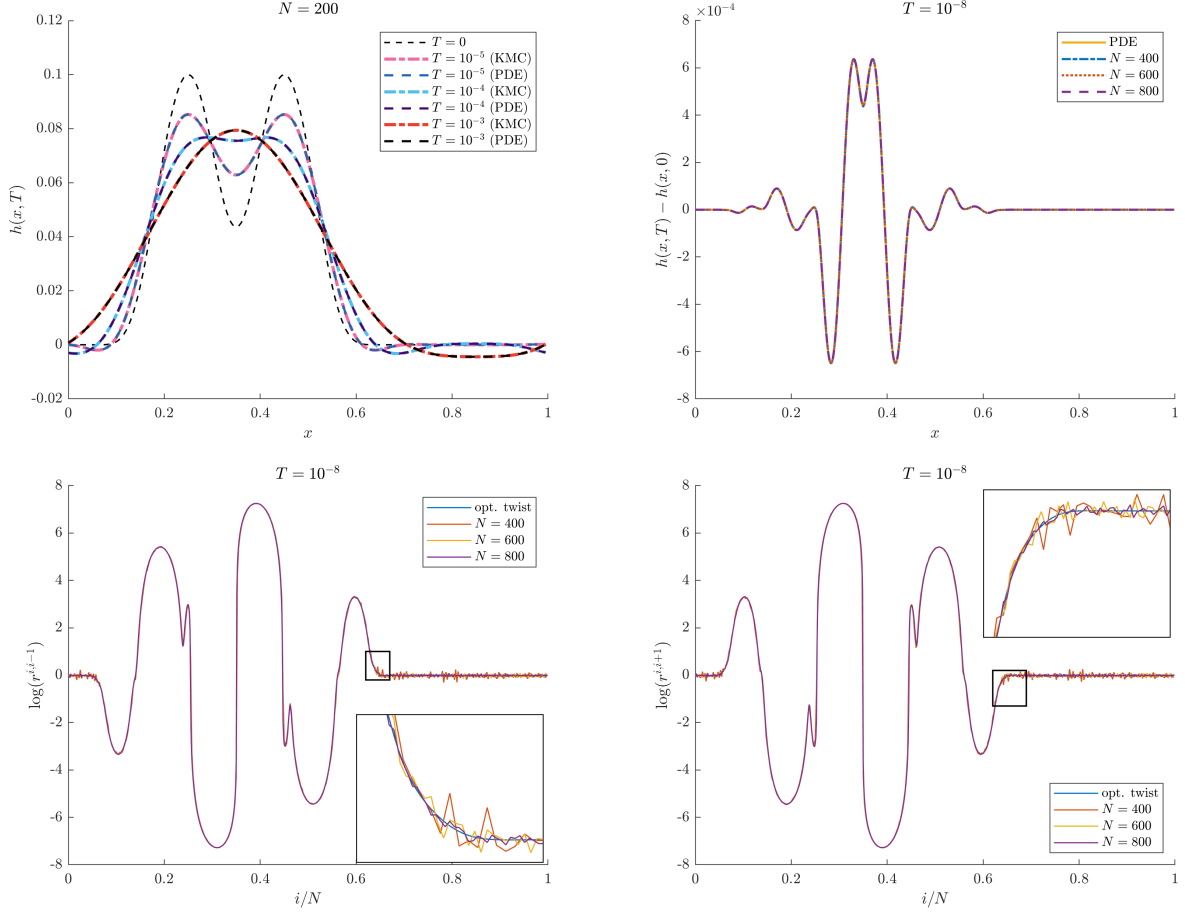


FIGURE 1. Metropolis rate dynamics with temperature $\beta = 0.01$, from initial profile $h(x, 0)$ given by a sum of a bump function $g(x)$ and its translation, $g(x + 0.2 \bmod 1)$. Top left: PDE vs KMC evolution with fixed N at various times T . Top right: PDE vs KMC short time evolution, $h(x, T) - h(x, 0)$, for fixed T and various N . Bottom left (bottom right): log of optimal twist average vs log of empirical average of rates to jump left (jump right) for fixed T and various N .

nearly converged. Thus the discrepancy between the PDE and microscopic profiles is not attributable to N being insufficiently large. Instead, it must be related to the optimal twist assumption. Indeed, the bottom plots show that the expected value of the rate observable is not given exactly by the expectation with respect to the optimal twist measure, though of course it is clearly a very close approximation to the actual measure.

Figure 3 shows results from the simulation of the Arrhenius rate dynamics with a sinusoidal initial profile and $\beta = 1.5$. We observe an excellent fit of the PDE solution to the microscopic profile, as seen in the top two figures. The bottom figures confirm the optimal twist assumption. Note that, for the purpose of a more readable display, we plot the logarithm of the jump rate averages for $i/N < 0.5$ in the bottom right figure and the rate averages themselves for $i/N > 0.5$ in the bottom left figure.

Discussion of the small discrepancy in Figure 2. Based on the bottom two plots in Figure 2, which show a discrepancy between the empirical rate expectation and the expectation under the optimal twist measure, it seems as though the optimal twist measure is not the exact local equilibrium measure for the Metropolis rate dynamics, though it is a good approximation. As mentioned above, the discrepancy is not a finite N error. It is also not due to the extra multiplicative factor $1 + 4e^{-\pi^2/\beta} \cos(\lambda_N^i \pi/\beta)$ mentioned in Remark 3.6, for including this factor does not eliminate the discrepancy.

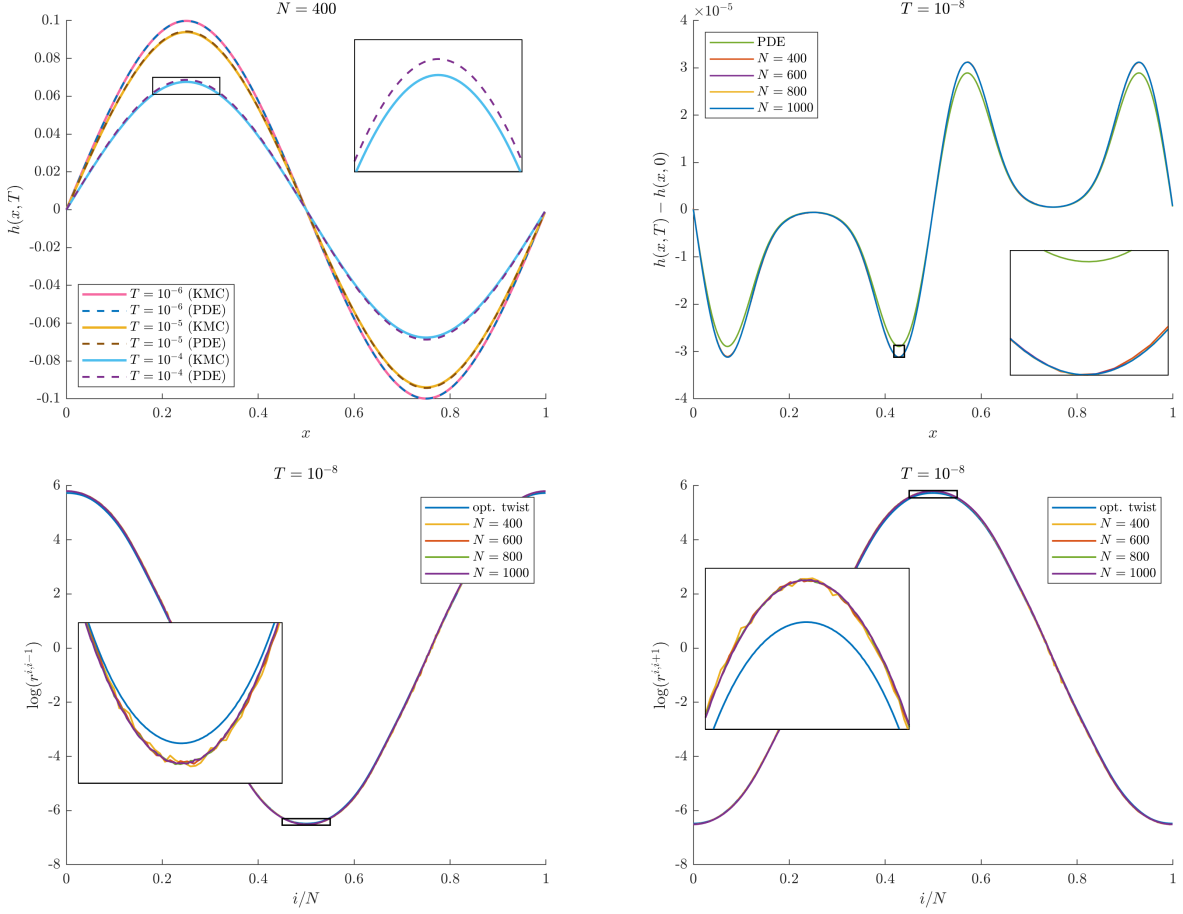


FIGURE 2. Metropolis rate dynamics with temperature $\beta = 0.25$, from initial profile $h(x, 0) = 0.1 \sin(2\pi x)$. Top left: PDE vs KMC evolution with fixed N at various times T . Top right: PDE vs KMC short time evolution, $h(x, T) - h(x, 0)$, for fixed T and various N . Bottom left (bottom right): optimal twist average vs empirical average of rates to jump left (jump right) for fixed T and various N .

The hypothesis that the optimal twist measure is not entirely accurate is supported by comparing our argument for the PDE derivation to that of [KDM95]. There, it is argued from physical principles that the macroscopic current, which we denote $\bar{\mathcal{J}}$, should be of the form

$$(31) \quad \bar{\mathcal{J}}(i/N, t) = \partial_{xx} \bar{\lambda}(i/N, t) \sigma(i/N, t), \quad \bar{\lambda}(x, t) = 2\beta \partial_x h(x, t).$$

In this equation, $\bar{\lambda}(x, t)$ is the macroscopic analog of what we call λ_i . The factor σ is the so-called mobility and $\sigma(i/N)$ is given by the sum of the expectation of the rate $r^{i, i+1}$ and an additional term, see equation (2.14) of [KDM95]. This additional term is identically zero for symmetric rates and generically nonzero.

In comparison, we obtain for the macroscopic current

$$\bar{\mathcal{J}}(i/N, t) = N^{q_2 - q_1 - 1} (1 - e^{-\lambda_{i-1} + 2\lambda_i - \lambda_{i+1}}) \langle r^{i, i+1} \rangle_{\lambda_N(t)}.$$

Recall that $\lambda_i \approx 2\beta N^{q_1 - 1} \partial_x h(i/N, t)$, so that $\lambda_{i-1} - 2\lambda_i + \lambda_{i+1} = O(N^{q_1 - 3})$. If $q_1 < 3$ and $q_2 = 4$ we obtain

$$N^{q_2 - q_1 - 1} (1 - e^{-\lambda_{i-1} + 2\lambda_i - \lambda_{i+1}}) \approx N^{3 - q_1} (\lambda_{i-1} - 2\lambda_i + \lambda_{i+1}) \approx \partial_{xx} \bar{\lambda}(i/N, t),$$

so that we can write the current as

$$(32) \quad \bar{\mathcal{J}}(i/N, t) \approx \partial_{xx} \bar{\lambda}(i/N, t) \langle r^{i, i+1} \rangle_{\lambda_N(t)}.$$

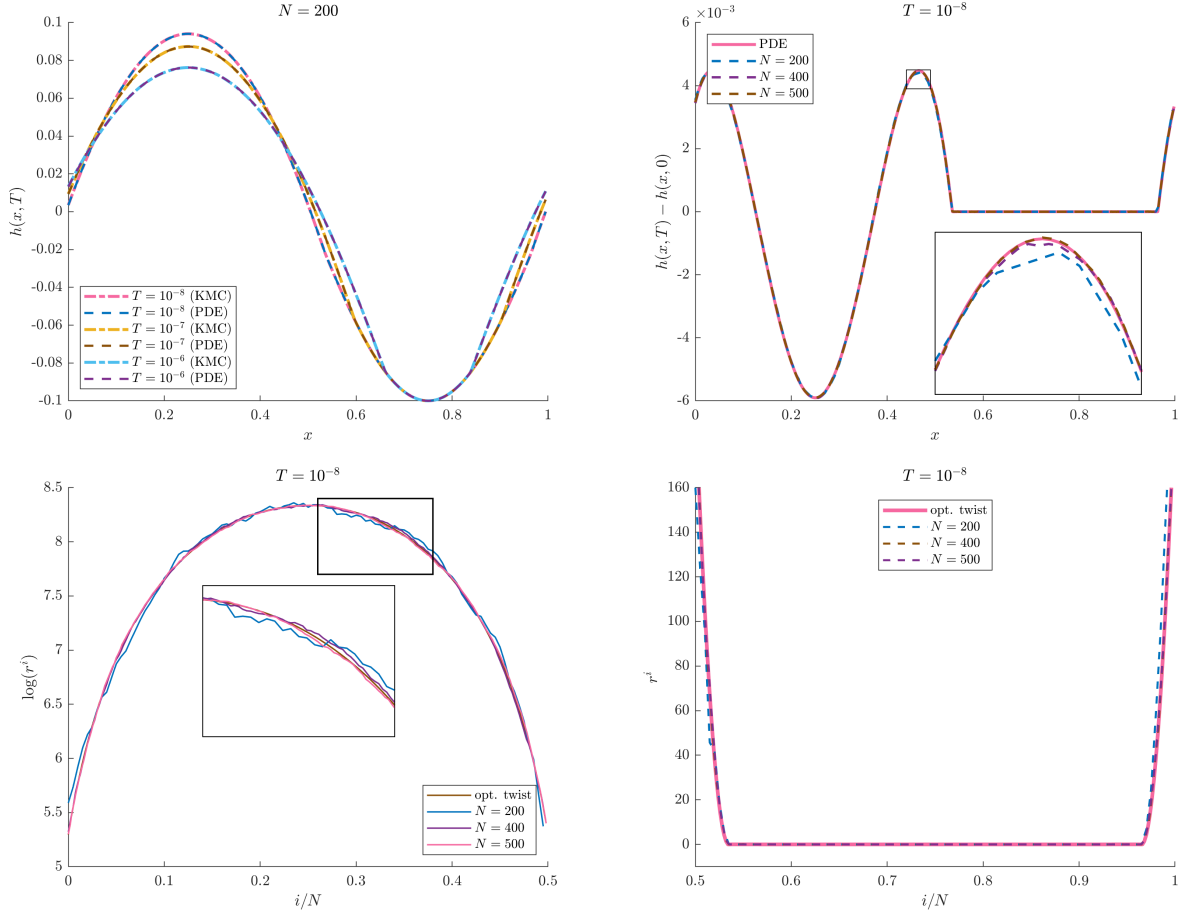


FIGURE 3. Arrhenius rate dynamics with temperature $\beta = 1.5$, from initial profile $h(x, 0) = 0.1 \sin(2\pi x)$. Top left: PDE vs KMC evolution with fixed N at various times T . Top right: PDE vs KMC short time evolution, $h(x, T) - h(x, 0)$, for fixed T and various N . Bottom: optimal twist average vs empirical average of rates, which are left/right symmetric. The bottom left is a plot of the logarithm of the jump rates at sites i with $i/N < 1/2$ (where rates are large). The bottom right is a plot of jump rates at sites i with $i/N > 1/2$ (where rates are close to zero)

Thus the two definitions of current, (31) and (32), are identical provided

$$\sigma(i/N, t) = \langle r^{i, i+1} \rangle_{\lambda_N(t)} + O(N^{-1}).$$

However, this is not the case for asymmetric rates, for which the second summand in the definition of the mobility does not vanish. This supports our belief that the optimal twist measure requires a correction. Note, however, that in order to compare our definition of current with that of [KDM95], we had to assume that $q_1 < 3$, which is not the case for the Metropolis rate dynamics. We leave further analysis of the validity of the optimal twist to future work.

4. GLOBAL SOLUTION AND LONG TIME DYNAMICS

In this section, we interpret the 4th order exponential PDE for Metropolis rate dynamics in Proposition 3.3 as a gradient flow of a proper convex functional with a L^2 dissipation. Then using the minimizing movement and the convergence analysis in [AGS08], we construct a global strong solution and prove there is no singularity formation. In Appendix B, we present ideas for another approach using the Bakry-Emery machinery.

After setting most physical constants to be 1, we obtain the continuous equation for surface growth with Metropolis-type rates

$$(33) \quad \partial_t u = \frac{1}{2} \partial_x [e^{-\partial_x^3 u} - e^{\partial_x^3 u}].$$

Denote $h := \partial_x u$. We obtain formally the equation for h

$$(34) \quad \partial_t h = \frac{1}{2} \partial_{xx} [e^{-\partial_{xx} h} - e^{\partial_{xx} h}] = -\partial_{xx} (\sinh(h_{xx})).$$

We will validate this equation by proving the global existence and the long time behavior of solutions to (34) with periodic boundary condition; see Theorem 4.6.

4.1. Gradient flow in $L^2(\mathbb{T})$. Let us first define formally a convex functional with some formal observations and recast (34) into a $L^2(\mathbb{T})$ gradient flow. Let ϕ be

$$(35) \quad \phi(h) := \int_{\mathbb{T}} \cosh(h_{xx}) \, dx.$$

The first variation of ϕ is

$$\frac{\delta \phi}{\delta h} = \partial_{xx} (\sinh(h_{xx}))$$

and then formally we have

$$(36) \quad h_t = -\frac{\delta \phi}{\delta h}.$$

To study the global strong solution to (34), we plan to apply the gradient flow theory in metric space $L^2(\mathbb{T})$. Let us first make some inspiring observations, which will be made rigorous in the proof later.

Observation 1 (Conservation Laws). Thanks to the periodic assumption, we have

$$(37) \quad \frac{d}{dt} \int_{\mathbb{T}} h \, dx = 0,$$

which implies $\int_{\mathbb{T}} h \, dx = \int_{\mathbb{T}} h_0 \, dx$. Moreover from $\int_{\mathbb{T}} h_{xx} \, dx = 0$, we know

$$(38) \quad \int_{\mathbb{T}} (h_{xx})^+ \, dx = \int_{\mathbb{T}} (h_{xx})^- \, dx.$$

Here $(h_{xx})^-$ is the negative part of h_{xx} and $(h_{xx})^+$ is the positive part of h_{xx} .

Observation 2 (Dissipation Inequalities). From the gradient flow structure (36),

$$(39) \quad \frac{d\phi}{dt} = \int_{\mathbb{T}} \frac{\delta \phi}{\delta h} h_t \, dx = - \int_{\mathbb{T}} \left| \frac{\delta \phi}{\delta h} \right|^2 \, dx = - \int_{\mathbb{T}} h_t^2 \, dx \leq 0,$$

which gives the observation

$$\phi(h(t)) \leq \phi(h(0)) \quad \text{for any } t \geq 0.$$

One shall notice the boundedness of functional ϕ gives us good estimates to prevent both the positive and negative parts of h_{xx} from becoming singular. Indeed, we have uniform estimate

$$\begin{aligned} \frac{1}{p} \int_{\mathbb{T}} (h_{xx}^+)^p \, dx &\leq \int_{\mathbb{T} \cap (h_{xx}^+ > 0)} e^{(h_{xx})^+} \, dx \leq \int_{\mathbb{T} \cap (h_{xx}^+ > 0)} \left(e^{(h_{xx})^+} + e^{-(h_{xx})^+} \right) \, dx \\ &\leq \int_{\mathbb{T}} (e^{h_{xx}} + e^{-h_{xx}}) \, dx = 2\phi(h(t)) \leq 2\phi(h(0)). \end{aligned}$$

Similarly, we have the same estimate for the negative part h_{xx}^- . Thus for any $p \in \mathbb{N}^+$,

$$(40) \quad \frac{1}{p} \int_{\mathbb{T}} |h_{xx}|^p \, dx \leq 4\phi(h(0)).$$

For simplicity we choose the working space

$$(41) \quad H := \left\{ u \in L^2(\mathbb{T}); \int_{\mathbb{T}} u \, dx = 0 \right\}, \quad V := \{ u \in H^2(\mathbb{T}); \int_{\mathbb{T}} u \, dx = 0 \}$$

with standard L^2 -norm, denoted as $\|\cdot\|$, and H^2 -norm, denoted as $\|\cdot\|_V$. Denote the best constant for Poincaré's inequality as $\kappa > 0$, which depends only on the size of the domain \mathbb{T} .

4.2. **Variational inequality solution.** Let ϕ be a functional

$$(42) \quad \phi : H \rightarrow [0, +\infty], \quad \phi(h) := \begin{cases} \int_{\mathbb{T}} \cosh(h_{xx}) \, dx & \text{if } h \in V; \\ +\infty & \text{otherwise.} \end{cases}$$

4.2.1. *Euler Scheme.* First let us establish the gradient flow evolution in the metric space (H, dist) , with distance $\text{dist}(u, v) := \|u - v\|$. Let $h_0(x) \in H$ be a given initial datum and $0 < \tau \ll 1$ be a given parameter. We consider a sequence $\{x_n^\tau\}$ which satisfies the following unconditional-stable backward Euler scheme

$$(43) \quad \begin{cases} x_n^{(\tau)} \in \operatorname{argmin}_{x' \in H} \left\{ \phi(x') + \frac{1}{2\tau} \|x' - x_{n-1}^{(\tau)}\|^2 \right\}, & n \geq 1, \\ x_0^{(\tau)} := h_0 \in H. \end{cases}$$

The existence and uniqueness of the sequence $\{x_n^\tau\}$ can be proved by direct methods in the calculus of variations after establishing the convexity and lower semicontinuity of ϕ in Proposition 4.2. Thus we consider the gradient descent with respect to ϕ in the space (H, dist) .

Now for any $0 < \tau \ll 1$ we define the resolvent operator, also known as proximal mapping of ϕ , (see [AGS08, p. 40])

$$\mathcal{J}_\tau[h] := \operatorname{argmin}_{v \in H} \left\{ \phi(v) + \frac{1}{2\tau} \|v - h\|^2 \right\},$$

then the variational approximation of h at t is obtained by Euler scheme (43) as

$$(44) \quad h_n(t) := (\mathcal{J}_{t/n})^n[h_0].$$

In Proposition 4.5, we will use the theory for gradient flow in metric space [AGS08, Theorem 4.0.4] to establish the convergence of the variational approximation $h_n(t)$ to variational inequality solution to (34), which is defined below.

Definition 4.1. *Given initial data $h_0 \in H$, we call $h : [0, +\infty) \rightarrow H$ a variational inequality solution to (34) if $h(t)$ is a locally absolutely continuous curve such that $\lim_{t \rightarrow 0} h(t) = h_0$ in H and*

$$(45) \quad \langle h_t(t), h(t) - v \rangle_{H', H} \leq \phi(v) - \phi(h(t)) \quad \text{for a.e. } t > 0, \forall v \in D(\phi).$$

Next we study some properties, including convexity and lower semicontinuity in H , of the functional ϕ .

4.3. **Convexity and lower semicontinuity of function ϕ in H .** We will prove the λ -convexity and lower semicontinuity of function ϕ in H . We note $\lambda > 0$ is important for the long time behavior of the global solution.

Proposition 4.2. *The functional $\phi : H \rightarrow [0, +\infty]$ is proper, λ -convex, lower semicontinuous in H and satisfies coercivity defined in [AGS08, (2.4.10)].*

Proof. Clearly since the typical function $h = Lx \in D(\phi)$, so $D(\phi) = \{\phi < +\infty\}$ is nonempty and ϕ is proper. Due to the positivity of ϕ , coercivity [AGS08, (2.4.10)], i.e., $\exists u^* \in D(\phi), r^* > 0$ such that $\inf\{\phi(v) : v \in H, \text{dist}(v, u^*) \leq r^*\} > -\infty$, is obvious.

λ -Convexity. Given $u, v \in H, t \in (0, 1)$, without loss of generality we assume $u, v \in D(\phi)$, otherwise the convexity inequality is trivial. Therefore from the definition of λ -convexity, we only need to prove for any $t \in [0, 1]$, any $u, v \in H$ we have

$$(46) \quad \phi((1-t)u + tv) \leq (1-t)\phi(u) + t\phi(v) - \frac{1}{2}\lambda t(1-t)\|u - v\|_{L^2}^2.$$

Denote

$$I(t) := \int_{\mathbb{T}} (1-t) \cosh(u_{xx}) + t \cosh(v_{xx}) - \frac{\lambda}{2} t(1-t) \|u - v\|_{L^2}^2 - \cosh((1-t)u_{xx} + tv_{xx}) \, dx$$

and notice $I(1) = I(0) = 0$. Thus we only need to prove $I''(t) \leq 0$. It is easy to calculate that

$$I''(t) = \int_{\mathbb{T}} -\cosh[(1-t)u_{xx} + tv_{xx}](v_{xx} - u_{xx})^2 + \lambda(u - v)^2 \, dx \leq \int_{\mathbb{T}} -(u_{xx} - v_{xx})^2 + \lambda(u - v)^2 \, dx \leq 0$$

due to Poincaré's inequality with $\lambda = \frac{1}{\kappa}$. Hence ϕ is λ -convex for $\lambda = \frac{1}{\kappa} > 0$.

Lower semicontinuity. Consider a sequence $h_n \rightarrow h$ in H . We need to check

$$\phi(h) \leq \liminf_n \phi(h_n).$$

If $h_n \in D(\phi)$ does not hold for all large n , then lower semicontinuity holds. Without loss of generality, we can assume $h_n \in D(\phi)$ for all n , and also

$$\liminf_n \phi(h_n) = \lim_n \phi(h_n).$$

First notice $h_n \in D(\phi)$ for any n implies uniform estimate

$$\begin{aligned} \frac{1}{p} \int_{\mathbb{T}} (h_{xx}^+)^p dx &\leq \int_{\mathbb{T} \cap \{h_{xx}^+ > 0\}} e^{(h_{xx})^+} dx \leq \int_{\mathbb{T} \cap \{h_{xx}^+ > 0\}} \left(e^{(h_{xx})^+} + e^{-(h_{xx})^+} \right) dx \\ &\leq \int_{\mathbb{T}} (e^{h_{xx}} + e^{-h_{xx}}) dx = 2\phi(h(t)) \leq 2\phi(h(0)). \end{aligned}$$

Similarly, we have the same estimate for the negative part h_{xx}^- . Thus for any $p = 2$,

$$(47) \quad \int_{\mathbb{T}} |h_{xx}|^2 dx \leq C,$$

which yields that there exists $h^* \in V$ such that $h_n \rightharpoonup h^*$ in V . From the strong convergence $h_n \rightarrow h$ in H we know the $h_n \rightharpoonup h$ in V . Therefore from the convexity of cosh function, we know ϕ is also convex in V and the lower semicontinuity w.r.t the weak topology of V

$$\liminf_n \phi(h_n) \geq \phi(h).$$

Thus the lower semicontinuity in H is proved. \square

As long as we have the convexity of ϕ , the $(\tau^{-1} + \lambda)$ -convexity is standard and the proof can be found in [AGS08, Section 2.4].

Proposition 4.3 ($(\tau^{-1} + \lambda)$ -convexity). *For any $h, v_0, v_1 \in D(\phi)$, there exists a curve $v : [0, 1] \rightarrow D(\phi)$ such that $v(0) = v_0$, $v(1) = v_1$ and the functional*

$$(48) \quad \Phi(\tau, h; v) := \phi(v) + \frac{1}{2\tau} \|h - v\|_H^2$$

satisfies τ^{-1} -convexity, i.e.,

$$(49) \quad \Phi(\tau, h; v(t)) \leq (1-t)\Phi(\tau, h; v_0) + t\Phi(\tau, h; v_1) - \frac{1}{2}(1/\tau + \lambda)t(1-t)\|v_0 - v_1\|_H^2$$

for all $\tau > 0$, $t \in [0, 1]$.

4.4. Existence and Long time behavior of global solution. After studying convexity and lower semicontinuity in last section, we shall apply the convergence result in [AGS08, Theorem 4.0.4] to derive that the discrete solution h_n obtained by Euler scheme (43) converges to the variational inequality solution defined in Definition 4.1. For $v \in D(\phi)$, denote the local slope

$$(50) \quad |\partial\phi|(v) := \limsup_{w \rightarrow v} \frac{\max\{\phi(v) - \phi(w), 0\}}{\text{dist}(v, w)}.$$

Remark 4.4. *In particular, by [AGS08, Proposition 1.4.4], we have the local slope is*

$$|\partial\phi|(v) = \min\{\|\xi\|; \xi \in \partial\phi(v)\}$$

for any $v \in H$. Since ϕ is a smooth functional, its subdifferential $\partial\phi$ is single-valued and equals its Frèchet differential

$$\partial\phi = D\phi(h) := [\sinh(h_{xx})]_{xx}.$$

Proposition 4.5. *Given $h_0 \in H$, for any $t > 0$, $t = n\tau$, let $h_n(t)$ defined in (44) be the approximation solution obtained by Euler scheme (43), then*

- (1) *There exists a local Lipschitz curve $h(t) : [0, +\infty) \rightarrow H \in MM(\Phi; h_0)$ (i.e. minimizing movement for Φ) such that*

$$(51) \quad h_n(t) \rightarrow h(t) \text{ in } L^2(\mathbb{T})$$

and $h : [0, +\infty) \rightarrow H$ is the unique EVI solution in the sense that h is unique among all the locally absolutely continuous curves such that $\lim_{t \rightarrow 0} h(t) = h_0$ in H and

$$(52) \quad \frac{1}{2} \frac{d}{dt} \|h(t) - v\|^2 + \frac{\lambda}{2} \|h(t) - v\|^2 \leq \phi(v) - \phi(h(t)), \quad \text{a.e. } t > 0, \forall v \in D(\phi);$$

- (2) *We have the following regularities*

$$(53) \quad \phi(h(t)) \leq \phi(v) + \frac{1}{2t} \|v - h_0\|_H^2, \quad \forall v \in D(\phi),$$

$$(54) \quad |\partial\phi|^2(h(t)) \leq |\partial\phi|^2(v) + \frac{1}{t^2} \|v - h_0\|_H^2, \quad \forall v \in D(|\partial\phi|);$$

- (3) *There exist $t_0 > 0$ and we have the exponential decay of $h(t)$*

$$(55) \quad \frac{\lambda}{2} \|h(t) - h^*\| \leq (\phi(h_0) - \phi(h^*)) e^{-2\lambda(t-t_0)}, \quad \text{for any } t \geq t_0 > 0,$$

where $h^* = 0$ is the unique minimizer of ϕ .

This Proposition is a direct result by combining [AGS08, Theorem 4.0.4] and [AGS08, Theorem 2.4.14] with Proposition 4.2 and Proposition 4.3.

Next by Proposition 4.2 and [AGS08, Theorem 2.4.15], we claim that given a better initial data h_0 , the EVI solution obtained above is a global strong solution to (34) with better properties as follows.

Theorem 4.6. *Given any $T > 0$ and initial datum $h_0 \in D(\partial\phi)$ such that $\phi(h_0) < +\infty$, the solution obtained in Proposition 4.5 is a global strong solution in the sense that $\partial_t h = -\partial\phi = -\partial_{xx}(\sinh(h_{xx}))$ holds for all $t \geq 0$ with the following regularities*

$$h \in C([0, T]; D(\partial\phi)) \cap C^1([0, T]; H)$$

and the decay estimate

$$(56) \quad \|h(t)\| \leq \|h_0\|, \quad \forall t \geq 0, \quad \|\partial_t h(t)\| = \|\partial\phi(h(t))\| \leq e^{-\lambda t} \|\partial\phi(h_0)\|_{L^2}, \quad \forall t \geq 0.$$

5. NUMERICS

In this section, we numerically explore some properties of the PDE (1). Due to the exponential dependence on $\beta \partial_{xx} h$ in (1), we are limited to the setting of either relatively high temperature (small β) or small curvature, in which case the PDE can be solved numerically. As in [MW13], we focus on two key phenomena: (a) wetting, or how compactly supported solutions evolve to fill the domain and (b) self-similar structures in the collapse to equilibrium. Similar numerical studies were undertaken in [MW13] for the Arrhenius rate PDE (2). While certainly not an exhaustive study of phenomena in these models, they are key features of the dynamics one would like to understand for the evolution of crystal surfaces.

5.1. Wetting. Motivated by properties of (2) shown in [MW13], one phenomenon we investigate for (1) is how quickly mass spreads from regions of non-zero height into regions with zero height. This process is known as wetting in the study of thin films. In order for facets (macroscopic flat regions on the crystal surface) to be stable features of a surface, the wetting rate should be finite. In Figure 4, we study this phenomenon for the PDE (1). Similar to (2), it appears numerically that the solution can wet at finite rate. One interesting difference between (1) and (2) is that for an initial nonnegative compactly supported profile, the numerical solution to (2) remains positive while the numerical solution to (1) dips below zero before levelling off. The wetting rate was investigated for the initial profile

$$(57) \quad h(0, x) = \begin{cases} e^{8-|x|^{-1} - (0.5-|x|)^{-1}} & \text{for } 0 < |x| < \frac{1}{2}, \\ 0 & \text{otherwise.} \end{cases}$$

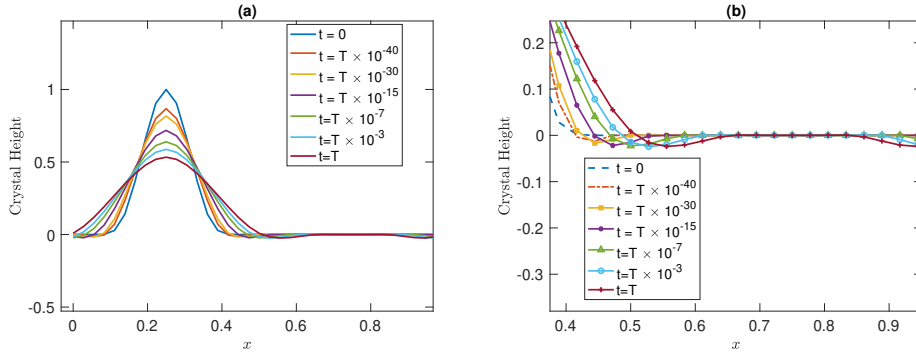


FIGURE 4. (Color online) Snapshots of solution of PDE (1) with $\beta = .05$, from the initial profile in (57), at various times in an interval of length $T = 5 \times 10^{-10}$ (a) and a blowup in the region of zero initial height (b).

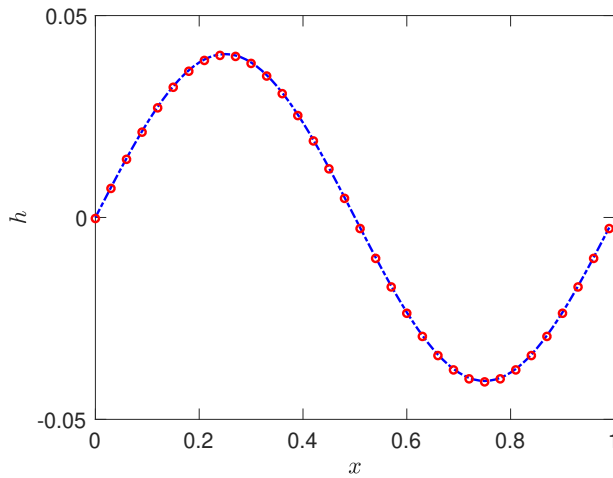


FIGURE 5. (Color online) Results of fixed-point iteration in which PDE (1) is evolved for some interval of time, then rescaled to have maximum height (in absolute value) equal to 1 and then evolved and rescaled repeatedly until convergence. The plot shows the last two fixed point iterations (before rescaling). The solution appears to be approximately of the form $h(t, x) = g(x)\phi(t)$. Here, we renormalize after intervals of length $T = 5e - 4$.

5.2. Self-Similarity. Again following the analysis in [MW13], we study the behavior of the surfaces as they near equilibrium ($h \equiv 0$). In Figure 5 we show that the surfaces appear to approximately factor as $h(t, x) = \phi(t)g(x)$ for very large t . The results in that figure are generated via a fixed point iteration in which the surface is evolved for some length of time and then rescaled so that the surface’s maximal (in absolute value) height is 1, and then evolved and rescaled repeatedly until convergence. The plot shows the last two fixed point iterations (before rescaling). The fact that they nearly coincide indicates that the iterations have converged to $g(x)$. We note that the function $g(x)$ will typically have some dependence on the particular initial profile. In this simulation we took $h(0, x) = \sin(2\pi x)$ and $\beta = .25$. It appears that the self-similar solution is quite regular. This is in contrast to (2), in which a singularity forms in the self-similar profile at its minimum.

APPENDIX A. SCALING LIMIT SUPPLEMENTARY PROOFS

We begin with a slightly more formal proof of our main proposition.

Proof of Proposition 3.3. We will show that h satisfies the PDE weakly, i.e that for all $\phi \in C_0^\infty(\mathbb{T})$, we have

$$(58) \quad \partial_t \int_0^1 \phi(x) h(x, t) dx = - \int_0^1 \phi'(x) \mathcal{D}h(x, t) dx,$$

where \mathcal{D} is given either by (19) or (20). By assumption of convergence, we have

$$(59) \quad \int_0^1 \phi(x) h(x, t + \epsilon) dx - \int_0^1 \phi(x) h(x, t) dx = \lim_{N \rightarrow \infty} \frac{1}{N} \sum_{j=0}^{N-1} \phi(j/N) N^{-q_1} (h_N^j(N^{q_2}(t + \epsilon)) - h_N^j(N^{q_2}t)).$$

Using equation (12) for the evolution of the microscopic process, we have

$$(60) \quad \begin{aligned} N^{-q_1} (h_N^i(N^{q_2}(t + \epsilon)) - h_N^i(N^{q_2}t)) &= N^{-q_1} \left(\int_{N^{q_2}t}^{N^{q_2}(t+\epsilon)} (\mathcal{A}\pi_i)(\mathbf{h}(s)) ds + M_i(N^{q_2}\epsilon) \right) \\ &= N^{q_2-q_1} \int_t^{t+\epsilon} (\mathcal{A}\pi_i)(\mathbf{h}(N^{q_2}s)) ds + N^{-q_1} M_i(N^{q_2}\epsilon). \end{aligned}$$

Here, $M_i(r), r \geq 0$ is a zero mean martingale with respect to the natural filtration generated by the random variables $\mathbf{h}(N^{q_2}t + r), r \geq 0$ conditioned on the value of $\mathbf{h}(N^{q_2}t)$. The integral in (60) is a (macroscopically) local time average and, assuming the onset of local equilibrium, can therefore be replaced with its expectation. Assuming Hypothesis 3.2, the distribution of the process is approximated by the optimal twist measure. Combined, these assumptions imply

$$\int_t^{t+\epsilon} (\mathcal{A}\pi_i)(\mathbf{h}(N^{q_2}s)) ds \approx \int_t^{t+\epsilon} \langle (\mathcal{A}\pi_i)(\mathbf{h}) \rangle_{\lambda_N(s)} ds =: I_N^i(t, \epsilon).$$

Substituting the right hand side of (60) into the right hand side of (59) and replacing the integral with $I_N^j(t, \epsilon)$, we obtain

$$\begin{aligned} \frac{1}{N} \sum_{j=0}^{N-1} \phi(j/N) N^{-q_1} (h_N^j(N^{q_2}(t + \epsilon)) - h_N^j(N^{q_2}t)) &= \\ N^{q_2-q_1} \frac{1}{N} \sum_{j=0}^{N-1} \phi(j/N) I_N^j(t, \epsilon) + N^{-q_1} \frac{1}{N} \sum_{j=0}^{N-1} \phi(j/N) M_j(N^{q_2}\epsilon). \end{aligned}$$

By the local equilibrium assumption, the local (in space) average of the martingale terms can be replaced by its expectation, which is zero. We therefore obtain

$$\int_0^1 \phi(x) h(x, t + \epsilon) dx - \int_0^1 \phi(x) h(x, t) dx = \lim_{N \rightarrow \infty} N^{q_2-q_1} \frac{1}{N} \sum_{j=0}^{N-1} \phi(j/N) I_N^j(t, \epsilon).$$

We now return to $I_N^i(t, \epsilon)$ and express it as a discrete derivative. We have

$$I_N^i(t, \epsilon) = \int_t^{t+\epsilon} \langle (\mathcal{A}\pi_i)(\mathbf{h}) \rangle_{\lambda_N(s)} ds = \int_t^{t+\epsilon} \langle \mathcal{J}^{i-1, i}(\mathbf{h}) \rangle_{\lambda_N(s)} ds - \int_t^{t+\epsilon} \langle \mathcal{J}^{i, i+1}(\mathbf{h}) \rangle_{\lambda_N(s)} ds,$$

where $\mathcal{J}^{i, i+1} = r^{i, i+1} - r^{i+1, i}$ is the instantaneous current from site i to site $i + 1$. Let

$$\mathcal{J}_N^{i, i+1}(t, \epsilon) = \int_t^{t+\epsilon} \langle \mathcal{J}^{i, i+1}(\mathbf{h}) \rangle_{\lambda_N(s)} ds,$$

so that $I_N^i(t, \epsilon) = \mathcal{J}_N^{i-1, i}(t, \epsilon) - \mathcal{J}_N^{i, i+1}(t, \epsilon)$. We then have

$$(61) \quad \begin{aligned} N^{q_2-q_1} \frac{1}{N} \sum_{j=0}^{N-1} \phi(j/N) I_N^j(t, \epsilon) &\approx N^{q_2-q_1-1} \frac{1}{N} \sum_{j=0}^{N-1} \phi'(j/N) \mathcal{J}_N^{j, j+1}(t, \epsilon) \\ &= \int_t^{t+\epsilon} \frac{1}{N} \sum_{j=0}^{N-1} \phi'(j/N) N^{q_2-q_1-1} \langle \mathcal{J}^{j, j+1}(\mathbf{h}) \rangle_{\lambda_N(s)} ds. \end{aligned}$$

From our argument in the main text, we know that for $q_1 = 2, q_2 = 4$ and Arrhenius rate dynamics,

$$N^{q_2 - q_1 - 1} \langle \mathcal{J}^{j, j+1}(\mathbf{h}) \rangle_{\lambda_N(s)} \approx (\mathcal{D}_{\text{Arr}} h)(j/N, s).$$

Thus the right hand side of (61) converges to

$$\int_t^{t+\epsilon} \int_0^1 \phi'(x) (\mathcal{D}_{\text{Arr}} h)(x, s) dx ds$$

as $N \rightarrow \infty$. Dividing by ϵ and taking $\epsilon \rightarrow 0$ gives the desired result. The argument for the Metropolis rate dynamics is the same. \square

Lemma A.1. *For any rates in detailed balance with the global equilibrium measure ρ_N , and for any measure p_λ in the optimal twist family, we have*

$$(62) \quad \langle \mathcal{J}^{i, i+1} \rangle_\lambda = (1 - \exp(-\lambda^{i-1} + 2\lambda^i - \lambda^{i+1})) \langle r^{i, i+1} \rangle_\lambda.$$

Proof. We may write $p_\lambda = \rho_N f_\lambda$, where ρ_N is the global equilibrium measure. Using this notation, we have

$$\langle \mathcal{J}^{i, i+1} \rangle_\lambda = \sum_{\mathbf{h}} r^{i, i+1}(\mathbf{h}) \rho_N(\mathbf{h}) f_\lambda(\mathbf{h}) - \sum_{\mathbf{h}} r^{i+1, i}(\mathbf{h}) \rho_N(\mathbf{h}) f_\lambda(\mathbf{h}).$$

Now, we can carry out the second summation over $J_i^{i+1} \mathbf{h}$ and reformulate the resulting summand using detailed balance and the fact that

$$f_\lambda(J_i^{i+1} \mathbf{h}) = \exp(-\lambda_{i-1} - 2\lambda_i + \lambda_{i+1}) f_\lambda(\mathbf{h}).$$

We have

$$r^{i+1, i}(J_i^{i+1} \mathbf{h}) \rho_N(J_i^{i+1} \mathbf{h}) f_\lambda(J_i^{i+1} \mathbf{h}) = \exp(-\lambda_{i-1} - 2\lambda_i + \lambda_{i+1}) r^{i, i+1}(\mathbf{h}) \rho_N(\mathbf{h}) f_\lambda(\mathbf{h}).$$

Substituting this expression and combining the two sums together, we obtain

$$\begin{aligned} \langle \mathcal{J}^{i, i+1} \rangle_\lambda &= (1 - \exp(-\lambda_{i-1} - 2\lambda_i + \lambda_{i+1})) \sum_{\mathbf{h}} r^{i, i+1}(\mathbf{h}) \rho_N(\mathbf{h}) f_\lambda(\mathbf{h}) \\ &= (1 - \exp(-\lambda^{i-1} + 2\lambda^i - \lambda^{i+1})) \langle r^{i, i+1} \rangle_\lambda. \end{aligned} \quad \square$$

Lemma A.2. *Let $m \in \mathbb{Z}$ and $z \in \mathbb{Z}$ be a random variable distributed according to p_λ , where $p_\lambda(n) \propto e^{-\beta n^2 + \lambda n}$. Then*

$$(63) \quad \langle e^{m\beta z} \rangle_\lambda = \begin{cases} e^{\beta m^2/4 + \lambda m/2}, & \text{if } m \text{ even,} \\ Z\left(\beta, \frac{\lambda}{2\beta}\right) e^{\beta m^2/4 + \lambda m/2} & \text{if } m \text{ odd,} \end{cases}$$

where

$$Z(\beta, \alpha) = \frac{\sum_{n=-\infty}^{\infty} e^{-\beta(n - (\alpha + \frac{1}{2}))^2}}{\sum_{n=-\infty}^{\infty} e^{-\beta(n - \alpha)^2}}.$$

If β is small, then $Z(\beta, \alpha) = 1 + O(\beta)$.

Proof. We have

$$(64) \quad \begin{aligned} \langle e^{m\beta z} \rangle_\lambda &= \frac{\sum_{n=-\infty}^{\infty} e^{m\beta n - \beta n^2 + \lambda n}}{\sum_{n=-\infty}^{\infty} e^{-\beta n^2 + \lambda n}} \\ &= \exp\left(\beta \left(\frac{m}{2} + \frac{\lambda}{2\beta}\right)^2\right) - \left(\frac{\lambda}{2\beta}\right)^2 \frac{\sum_{n=-\infty}^{\infty} e^{-\beta(n - (\frac{m}{2} + \frac{\lambda}{2\beta}))^2}}{\sum_{n=-\infty}^{\infty} e^{-\beta(n - \frac{\lambda}{2\beta})^2}}. \end{aligned}$$

The factor in front of the ratio of sums simplifies to

$$e^{\beta m^2/4 + \lambda m/2}.$$

If m is even then, by summing over $n - \frac{m}{2}$, we see that the numerator of the sum ratio equals the denominator. If m is odd, we can sum over $n - \frac{m-1}{2}$ in the numerator to obtain

$$\frac{\sum_{n=-\infty}^{\infty} e^{-\beta(n - \frac{1}{2} - \frac{\lambda}{2\beta})^2}}{\sum_{n=-\infty}^{\infty} e^{-\beta(n - \frac{\lambda}{2\beta})^2}}.$$

To see that $Z(\beta, \alpha) = 1 + O(\beta)$ one can express the sums in terms of the Jacobi theta function ϑ_3 and use properties of this function. \square

Using Lemma A.2, we can now compute the expectation $\langle r^{i,i+1} \rangle_\lambda$ for the Metropolis and Arrhenius rates.

Proposition A.3. *For the Arrhenius rates,*

$$\langle r_{Arr}^{i,i+1} \rangle_\lambda = \frac{1}{2} \exp(-(\lambda^i - \lambda^{i-1})).$$

For the Metropolis rates,

$$\langle r_{Met}^{i,i+1} \rangle_\lambda = e^{-\frac{3}{2}\beta} \exp\left(\frac{1}{2}(\lambda^{i-1} - 2\lambda^i + \lambda^{i+1})\right) Z(\beta, \lambda^{i-1}/2\beta) Z(\beta, \lambda^{i+1}/2\beta).$$

Proof. We use the form of the rates in (8) and (10), given by a product of exponential terms of the form e^{mz_i} . Assuming that we induce negligible error by taking the z_i 's to be independent under the optimal twist, we can express the expectation of this product as a product of expectations. For Arrhenius rates,

$$\langle r^{i,i+1} \rangle_\lambda = \frac{1}{2} e^{-2\beta} \langle e^{-2\beta z} \rangle_{\lambda^i} \langle e^{2\beta z} \rangle_{\lambda^{i-1}} = \frac{1}{2} e^{-2\beta} e^{\beta - \lambda^i} e^{\beta + \lambda^{i-1}} = \frac{1}{2} \exp(-(\lambda^i - \lambda^{i-1})).$$

For Metropolis rates,

$$\begin{aligned} \langle r^{i,i+1} \rangle_\lambda &= e^{-3\beta} \langle e^{\beta z} \rangle_{\lambda^{i-1}} \langle e^{-2\beta z} \rangle_{\lambda^i} \langle e^{\beta z} \rangle_{\lambda^{i+1}} \\ &= e^{-3\beta} e^{\beta/4 + \lambda^{i-1}/2} e^{\beta - \lambda^i} e^{\beta/4 + \lambda^{i+1}/2} Z(\lambda^{i-1}, \beta) Z(\lambda^{i+1}, \beta) \\ &= e^{-\frac{3}{2}\beta} \exp\left(\frac{1}{2}(\lambda^{i-1} - 2\lambda^i + \lambda^{i+1})\right) Z(\lambda^{i-1}, \beta) Z(\lambda^{i+1}, \beta). \end{aligned} \quad \square$$

APPENDIX B. ANOTHER METHOD FOR LONG TIME BEHAVIOR BY BAKRY-EMERY STRATEGY

Since ϕ is a smooth functional, its subdifferential $\partial\phi$ is single-valued and equals its Fréchet differential $\partial\phi(h) = [\sinh(h_{xx})]_{xx}$. We give another simple proof for the exponential decay to 0 of the global classical solution h .

On one hand, it is easy to obtain the energy dissipation

$$(65) \quad \frac{d\phi}{dt} = \int \partial\phi(h) h_t dx = \int -|\partial\phi|^2 dx =: D.$$

On the other hand, we use the λ -convexity of ϕ to establish the connection between D and ϕ . First, from the λ -convexity (46) with some $\lambda > 0$, we know $\phi(h) - \frac{\lambda}{2}\|h\|^2$ is convex. Thus we have

$$(66) \quad \phi(h(t)) - \frac{\lambda}{2}h^2(t) - \phi(v) + \frac{\lambda}{2}v^2 \leq \langle \partial\phi(h(t)), h(t) - v \rangle$$

for any $v \in L^2$. Then we obtain

$$(67) \quad \phi(h(t)) - \phi(v) \leq -\frac{\lambda}{2}\|h - v\|^2 + \langle \partial\phi(h(t)), h(t) - v \rangle$$

for any $v \in L^2$. Using Young's inequality, we have

$$(68) \quad \langle \partial\phi(h(t)), h(t) - v \rangle \leq \frac{\lambda}{2}\|h - v\|^2 + \frac{1}{2\lambda}\|\partial\phi\|^2.$$

From this, the estimate (67) becomes

$$(69) \quad \phi(h(t)) - \phi(v) \leq -\frac{\lambda}{2}\|h - v\|^2 + \langle \partial\phi(h(t)), h(t) - v \rangle \leq \frac{1}{2\lambda}\|\partial\phi\|^2.$$

Combining (69) with (65), we obtain

$$(70) \quad \frac{d}{dt}(\phi(h(t)) - \inf \phi) = -\|\partial\phi\|^2 \leq -2\lambda(\phi(h(t)) - \inf \phi),$$

which gives the exponential decay to $\inf \phi = \phi(h^*)$ with $h^* = 0$, i.e.

$$(71) \quad \phi(h(t)) - \phi(h^*) \leq (\phi(h(0)) - \phi(h^*))e^{-2\lambda t}.$$

REFERENCES

- [AGS08] Luigi Ambrosio, Nicola Gigli, and Giuseppe Savaré. *Gradient flows: in metric spaces and in the space of probability measures*. Springer Science & Business Media, 2008.
- [Bin83] Vu Thien Binh. Surface mobilities on solid materials. Technical report, Plenum Publishing Corp., New York, NY, 1983.
- [GLL19] Yuan Gao, Jian-Guo Liu, and Xin Yang Lu. Gradient flow approach to an exponential thin film equation: global existence and latent singularity. *ESAIM: Control, Optimisation and Calculus of Variations*, 25:49, 2019.
- [GLLM19] Yuan Gao, Jian-Guo Liu, Jianfeng Lu, and Jeremy L Marzuola. Analysis of a continuum theory for broken bond crystal surface models with evaporation and deposition effects. *arXiv preprint arXiv:1905.00179*, 2019.
- [KDM95] J Krug, HT Dobbs, and S Majaniemi. Adatom mobility for the solid-on-solid model. *Zeitschrift für Physik B Condensed Matter*, 97(2):281–291, 1995.
- [KMV03] M. Katsoulakis, A. Majda, and D. Vlachos. Coarse-grained stochastic processes and Monte Carlo simulations in lattice systems. *Journal of Computational Physics B*, 186:250–278, 2003.
- [LLMM19] Jian-Guo Liu, Jianfeng Lu, Dionisios Margetis, and Jeremy L Marzuola. Asymmetry in crystal facet dynamics of homoepitaxy by a continuum model. *Phys. D*, 393:54–67, 2019.
- [LX16] Jian-Guo Liu and Xiangsheng Xu. Existence theorems for a multidimensional crystal surface model. *SIAM Journal on Mathematical Analysis*, 48(6):3667–3687, 2016.
- [LX17] Jian-Guo Liu and Xiangsheng Xu. Analytical validation of a continuum model for the evolution of a crystal surface in multiple space dimensions. *SIAM Journal on Mathematical Analysis*, 49(3):2220–2245, 2017.
- [MW13] Jeremy L. Marzuola and Jonathan Weare. Relaxation of a family of broken-bond crystal-surface models. *Phys. Rev. E*, 88:032403, Sep 2013.
- [PV98] Alberto Pimpinelli and Jacques Villain. *Physics of crystal growth*, volume 19. Cambridge university press Cambridge, 1998.
- [Xu18] Xiangsheng Xu. Existence theorems for a crystal surface model involving the Δ -laplace operator. *SIAM Journal on Mathematical Analysis*, 50(4):4261–4281, 2018.

DEPARTMENT OF MATHEMATICS, DUKE UNIVERSITY, DURHAM, NC 27708
E-mail address: yuangao@math.duke.edu

COURANT INSTITUTE OF MATHEMATICAL SCIENCES, NEW YORK UNIVERSITY, 251 MERCER STREET, NEW YORK, NY 10012, USA
E-mail address: katsevich@cims.nyu.edu

DEPARTMENT OF MATHEMATICS AND DEPARTMENT OF PHYSICS, DUKE UNIVERSITY, DURHAM, NC 27708
E-mail address: jliu@math.duke.edu

DEPARTMENT OF MATHEMATICS, DEPARTMENT OF PHYSICS, AND DEPARTMENT OF CHEMISTRY, DUKE UNIVERSITY, DURHAM, NC 27708
E-mail address: jianfeng@math.duke.edu

DEPARTMENT OF MATHEMATICS, UNC-CHAPEL HILL, CB#3250 PHILLIPS HALL, CHAPEL HILL, NC 27599
E-mail address: marzuola@math.unc.edu